Plotting Isoclinics for Hybrid Photoelasticity and Finite Element Analysis

by M. Ragulskis and L. Ragulskis

ABSTRACT—Displacement-based finite element method formulations are coupled with stress-based photoelasticity analysis. As the stress field is discontinuous at the interelement boundaries, the introduced smoothing procedure enables the generation of high-quality digital images acceptable for hybrid experimental–numerical techniques. The proposed methods are applicable for the analysis of static and dynamic results of experimental photoelasticity.

KEY WORDS—Photoelasticity, finite element analysis, isoclinics

Introduction

Photoelasticity is one of the oldest methods for experimental stress analysis, but has been overshadowed by the finite element method (FEM) for engineering applications over the past three decades. However, new developments and applications, such as infrared photoelasticity, low-cost dynamic photoelasticity, photoelastic applications in stereolithography, etc., have revived the use of photoelasticity.[1–3] In particular, the determination of the stress concentration in front of notches and holes was, and still is, one of the most common applications of photoelasticity in the design of machine elements.

The principles of photoelasticity are well known.[4,5] The standard plane polariscope consists of the light source and a pair of polarizers, called a polarizer and an analyzer, with crossed polarization axes on either side of the model. The largest drawback of the method of photoelasticity is the complexity of the calculation procedures for the components of stresses from optical isoclinic lines and isochromatic fringe patterns. The produced optical patterns must be analyzed using complicated finite difference approaches.[5,6]

Visualization of the results from finite element analysis (FEA) procedures is important for several reasons. The first reason is the meaningful and accurate representation of processes taking place in the analyzed structures.[7] The second, and perhaps even more important, reason is preparing the ground for hybrid numerical–experimental techniques. Examples of FEM applications in developing hybrid techniques are readily available.[8] Unfortunately, conventional FEA techniques are based on the approximation of nodal displacements (not stresses) via the shape functions.[9–11] Ramesh and Pathak[12] have correctly noted that photoelastic isochromatics can be effectively used for the detection of FEM meshing problems.

A conventional FEM would require unacceptably dense meshing for producing sufficiently smooth photoelastic patterns. Multiscale meshing is not affordable either; the whole domain of the structure must be analyzed with the same accuracy. Therefore, there exists a need for the development of a technique for smoothing the generated photoelastic fringe patterns representing the stress distribution and calculated from the displacement distribution. The proposed smoothing technique is based on conjugate approximations used for the calculation of nodal values of stresses[9] and provides digital images of acceptable quality on relatively rather coarse meshes. The hybrid FEM[13] based on the interpolation of stresses (not displacements) cannot be effectively used, as the calculation of the eigenmodes would be practically impossible due to the complexity of formulations.

The purpose of this paper is the development of techniques for hybrid experimental–numerical photoelasticity analyses. The general scheme of such analyses is presented in Fig. 1. The generation of digital images mimicking the effect of photoelasticity naturally incorporates into the hybrid iterative procedure enabling effective interpretation of experimental results and provides insight into the physical processes taking place in the analyzed objects.

Construction of the Digital Photoelastic Images

Initial data for the construction of the digital photoelastic images are nodal values of displacements produced by finite element calculations. If the analysis of a dynamical process is considered, the eigenmodes for the structure in the state of plane stress are calculated by using the displacement formulation common in the FEA. It is assumed that the structure experiences high-frequency vibrations according to the eigenmode (the frequency of excitation is about equal to the eigenfrequency of the corresponding eigenmode and the eigenmodes are not multiple). The loading scheme of the analyzed cantilever plate is illustrated in Fig. 2.

The production of photoelastic images from finite element results requires the nodal values of the components of stresses. It can be noted that the calculation of these values is not a trivial procedure in conventional FEA based on displacement formulation.

M. Ragulskis (minvydas.ragulskis@ktu.lt) is a Professor, Department of Mathematical Research in Systems, Kaunas University of Technology, Studentu 50-222, LT-51368 Kaunas, Lithuania. L. Ragulskis is a Research Associate, Department of Informatics, Vytautas Magnus University, Vileikos 8, LT-44404 Kaunas, Lithuania.

Original manuscript submitted: July 3, 2002.
Final manuscript received: February 12, 2004.
DOI: 10.1177/0014485104044315

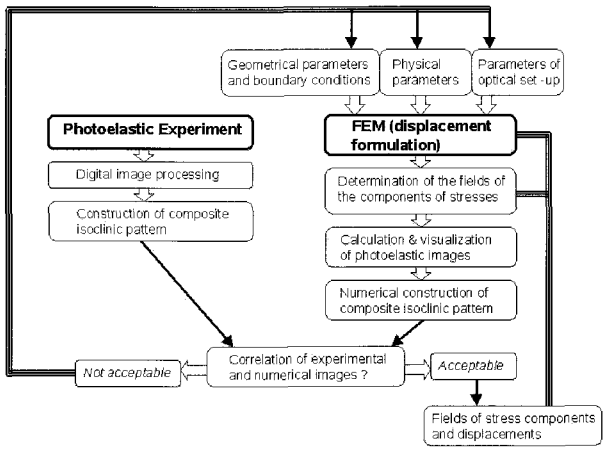

Fig. 1—Procedure of hybrid experimental–numerical analysis

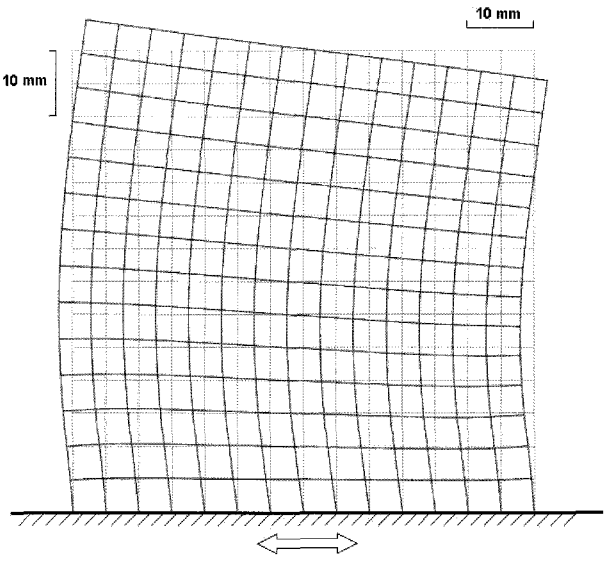

Fig. 2—Third eigenmode of the cantilever plate: gray lines, the structure in equilibrium; black lines, the eigenmode

The components of stresses in the domain of the analyzed finite element can be calculated in the usual way

$$\begin{Bmatrix} \sigma_x \\ \sigma_y \\ \tau_{xy} \end{Bmatrix} = [D][B]\{\delta_0\}, \tag{1}$$

where $\{\delta_0\}$ is the vector of nodal displacements of the eigenmode, $[B]$ is the matrix relating the strains with the displacements, $[D]$ is the matrix relating the stresses with the strains, and σ_x, σ_y, and τ_{xy} are the components of the stresses in the problem of plane stress. It can be noted that the displacements are continuous at interelement boundaries, but the calculated stresses are discontinuous due to the operation of differentiation.

The most natural way for the calculation of the nodal values of stresses is the minimization of the squared difference between the continuous strain function (eq (1)) and the interpolated stress field by the form functions of the analyzed element. Moreover, those differences are integrated in the domains of appropriate elements:

$$\begin{aligned} &\sum_i \tfrac{1}{2} \iint_{e_i} \left([N]\{\delta_x\} - \sigma_x\right)^2 \mathrm{d}x\,\mathrm{d}y, \\ &\sum_i \tfrac{1}{2} \iint_{e_i} \left([N]\{\delta_y\} - \sigma_y\right)^2 \mathrm{d}x\,\mathrm{d}y, \\ &\sum_i \tfrac{1}{2} \iint_{e_i} \left([N]\{\delta_{xy}\} - \tau_{xy}\right)^2 \mathrm{d}x\,\mathrm{d}y. \end{aligned} \tag{2}$$

Here, $\{\delta_x\}$ is the vector of nodal values of σ_x, $\{\delta_y\}$ is the vector of nodal values of σ_y, $\{\delta_{xy}\}$ is the vector of nodal values of τ_{xy}, $[N]$ is the row of the shape functions of the finite element, and e_i denotes the domain of the ith finite element; summation denotes the direct stiffness procedure.[11]

Unfortunately, the solution of unknown nodal values $\{\delta_x\}$, $\{\delta_y\}$, and $\{\delta_{xy}\}$ from eq (2) is unsatisfactory for the generation of digital photoelastic images, as the derivatives of the interpolated stress fields are still discontinuous. This is illustrated in the numerical results. Therefore, additional penalty terms for fast variation of the stress fields are introduced

$$\begin{aligned} &\lambda\left(\left(\frac{\partial\sigma_x}{\partial x}\right)^2 + \left(\frac{\partial\sigma_x}{\partial y}\right)^2\right), \\ &\lambda\left(\left(\frac{\partial\sigma_y}{\partial x}\right)^2 + \left(\frac{\partial\sigma_y}{\partial y}\right)^2\right), \\ &\lambda\left(\left(\frac{\partial\tau_{xy}}{\partial x}\right)^2 + \left(\frac{\partial\tau_{xy}}{\partial y}\right)^2\right), \end{aligned} \tag{3}$$

where λ is a parameter of smoothing. Trivial transformations lead to

$$\begin{aligned} &\sum_i \tfrac{1}{2} \iint_{e_i} \Big(\left([N]\{\delta_x\} - \sigma_x\right)^2 \\ &\quad + \lambda \{\delta_x\}^{\mathrm{T}} \left[B^*\right]^{\mathrm{T}} \left[B^*\right] \{\delta_x\}\Big) \mathrm{d}x\,\mathrm{d}y, \\ &\sum_i \tfrac{1}{2} \iint_{e_i} \Big(\left([N]\{\delta_y\} - \sigma_y\right)^2 \\ &\quad + \lambda \{\delta_y\}^{\mathrm{T}} \left[B^*\right]^{\mathrm{T}} \left[B^*\right] \{\delta_y\}\Big) \mathrm{d}x\,\mathrm{d}y, \\ &\sum_i \tfrac{1}{2} \iint_{e_i} \Big(\left([N]\{\delta_{xy}\} - \tau_{xy}\right)^2 \\ &\quad + \lambda \{\delta_{xy}\}^{\mathrm{T}} \left[B^*\right]^{\mathrm{T}} \left[B^*\right] \{\delta_{xy}\}\Big) \mathrm{d}x\,\mathrm{d}y, \end{aligned} \tag{4}$$

where $[B^*]$ is the matrix of the derivatives of the shape functions (the first row with respect to x; the second row with respect to y). The minimization of residuals defined by eq (4) leads to the following systems of linear algebraic equations for the determination of each of the component of the stresses:

$$\begin{aligned} &\left(\sum_i \iint_{e_i} \left([N]^{\mathrm{T}}[N] + \left[B^*\right]^{\mathrm{T}} \lambda \left[B^*\right]\right) \mathrm{d}x\,\mathrm{d}y\right) \\ &\quad \cdot \{\delta_x\} = \sum_i \iint_{e_i} [N]^{\mathrm{T}} \sigma_x \mathrm{d}x\,\mathrm{d}y, \\ &\left(\sum_i \iint_{e_i} \left([N]^{\mathrm{T}}[N] + \left[B^*\right]^{\mathrm{T}} \lambda \left[B^*\right]\right) \mathrm{d}x\,\mathrm{d}y\right) \\ &\quad \cdot \{\delta_y\} = \sum_i \iint_{e_i} [N]^{\mathrm{T}} \sigma_y \mathrm{d}x\,\mathrm{d}y, \\ &\left(\sum_i \iint_{e_i} \left([N]^{\mathrm{T}}[N] + \left[B^*\right]^{\mathrm{T}} \lambda \left[B^*\right]\right) \mathrm{d}x\,\mathrm{d}y\right) \\ &\quad \cdot \{\delta_{xy}\} = \sum_i \iint_{e_i} [N]^{\mathrm{T}} \tau_{xy} \mathrm{d}x\,\mathrm{d}y. \end{aligned} \tag{5}$$

It can be noted that when the parameter of smoothing is too small the reconstructed images are of unacceptable quality because of the non-physical behavior of the stress field as a result of its calculation from the displacement formulation. When the parameter is too big an oversmoothed image is obtained, which may look acceptable but is far from the real photoelastic image. The selection of the smoothing parameter λ can be performed using the error norms[10] of the finite elements. The components of the stresses can be interpolated from their nodal values by using the shape functions of the finite element. Then the components of strains ε_x ε_y, and γ_{xy} are obtained using those values of stresses and the matrix of elastic constants:

$$\{\varepsilon\} = \begin{Bmatrix} \varepsilon_x \\ \varepsilon_y \\ \gamma_{xy} \end{Bmatrix} = [D]^{-1} \begin{Bmatrix} \sigma_x \\ \sigma_y \\ \tau_{xy} \end{Bmatrix}. \tag{6}$$

The relative error norm for the ith finite element can then be calculated as

$$\psi_i = \frac{\iint\limits_{e_i} (\{\varepsilon\} - [B]\{\delta_0\})^{\mathrm{T}} [D] (\{\varepsilon\} - [B]\{\delta_0\}) \, dx \, dy}{\iint\limits_{e_i} \{\varepsilon\}^{\mathrm{T}} [D] \{\varepsilon\} \, dx \, dy}. \tag{7}$$

For those parts of the image where the relative error norms of the finite elements are too large, the image is expected to be of insufficient quality, and a finer meshing or smoothing of the image with a larger value of the smoothing parameter may be required. The selection of smoothing parameter λ is then straightforward

$$\lambda = f\left(\sum_i \psi_i\right) \tag{8}$$

where function f can be selected as a linear growing function, $f(0) = 0$. The slope of the function depends on the meshing and particularly the type of the finite element used.

The principal stresses σ_1 and σ_2 at each node are calculated as the eigenvalues of the matrix

$$\begin{bmatrix} \sigma_x & \tau_{xy} \\ \tau_{xy} & \sigma_y \end{bmatrix}, \tag{9}$$

and the normalized eigenvectors of this matrix $\{V_1\}$ and $\{V_2\}$ are the directions of the principal stresses.

The vector of polarization is assumed to be given as

$$\{P\} = \begin{Bmatrix} \cos\alpha \\ \sin\alpha \end{Bmatrix}, \tag{10}$$

where α is the angle of the vector of polarization with the x-axis.

Then the intensity in the photoelastic image of the plane polariscope (isoclinics and isochromatics intertwined) is calculated as

$$I = (([V_1] \cdot \{P\}) ([V_2] \cdot \{P\}) \sin C (\sigma_1 - \sigma_2))^2, \tag{11}$$

where C is the constant dependent on the thickness of the analyzed structure in the state of plane stress and on the material from which it is produced.[4,5]

The intensity of the photoelastic image for the circular polariscope (isochromatics) is calculated as

$$I = (\sin C (\sigma_1 - \sigma_2))^2, \tag{12}$$

and the intensity of the isoclinics pattern is calculated as

$$I = (([V_1] \cdot \{P\}) ([V_2] \cdot \{P\}))^2. \tag{13}$$

It can be noted that the latter image cannot be obtained directly from the experimental investigations but is required for the determination of the stress field.

The relationships presented above form the basis for the generation of digital photoelastic images. The procedure of construction of digital images in projection planes from isoparametric finite elements is described in detail elsewhere.[15]

Numerical Results

A rectangular, cantilevered plate with fixed edge, in a state of plane stress, is analyzed. The lower edge of the plate is fastened (both components of displacements are assumed equal to zero). It is considered that the plate is experiencing resonant vibrations on an eigenmode that is not multiple; the loading is assumed to be harmonic with the frequency of the eigenmode and not orthogonal to it. The motion according to a single eigenmode is analyzed. The third eigenmode of the plate and the loading scheme are shown in Fig. 2. The reconstructed principal stresses (the eigenmode of stresses) at the nodes are shown in Fig. 3(a). The isolines of the absolute value of the difference of the principal stresses are presented in Fig. 3(b). The principal directions of the stresses are shown in Fig. 3(c). The reconstructed image for the circular polariscope (isochromatics) is shown in Fig. 4.

The directions of the principal stresses are directly related with the images presented further. The images of the isoclines at $\alpha = 0$ and the corresponding image for the plane polariscope (isoclinics and isochromatics intertwined) are presented in Figs. 5(a) and (b), respectively. The corresponding images at $\alpha = \pi/8$ are shown in Figs. 6(a) and (b). Finally, the isolines of the principal directions of the stresses corresponding to the darkest parts from the images of the isoclines (pattern of isoclinics) are shown in Fig. 7. The numbers in Fig. 7 are related to the angle of the vector of polarization with the x-axis, α. The consecutive numbers $i = 1, \ldots, 10$ correspond to the values of $\alpha = \frac{(i-1)\pi}{20}$.

Another important numerical procedure is the determination of the isotropic points in the isoclinic pattern.[5] An isotropic point is the point through which all isoclinics pass. Isotropic points are important for experimental stress analysis when determining zero-order isochromatic fringes. The results in Table 1 represent the relationship between the number of the eigenmode and the number of isotropic points in the analyzed rectangular plate. It can be seen that the complexity of the stress field increases with the number of the eigenmode.

It can be noted that the presented methodology can also be applied to static FEA. Digital photoelastic images are constructed for a disk in diametral compression under constant load. The loading scheme and the pattern of isoclinics are presented in Fig. 8(a). Unsmoothed isochromatics are shown in Fig. 8(b). This picture clearly illustrates the importance of the presented smoothing procedure. The selection of an

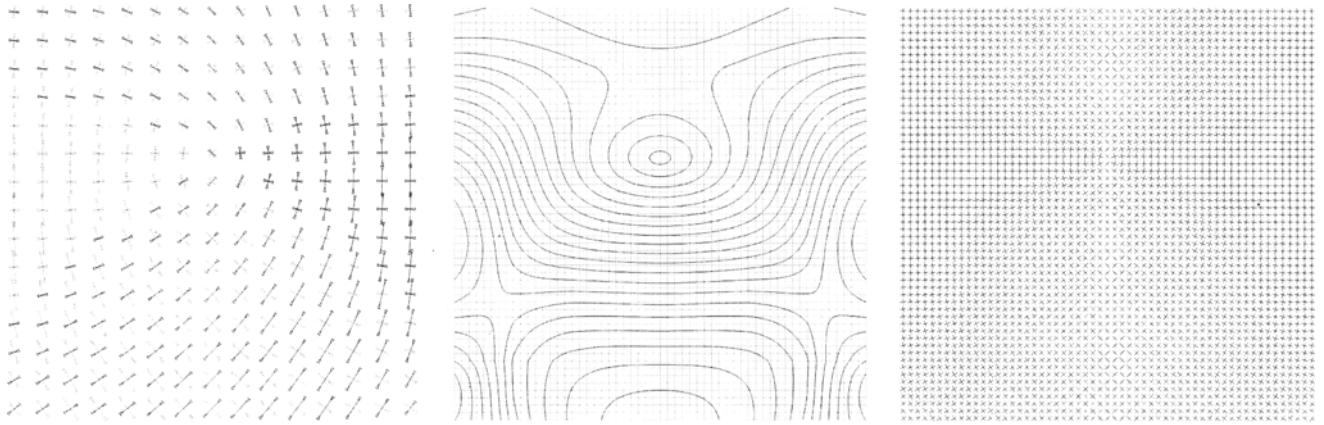

Fig. 3—(a) Reconstructed nodal principal stresses of the third eigenmode (dark gray, negative; light gray, positive). (b) The isolines of the absolute value of the difference of the principal stresses of the third eigenmode. (c) The principal directions of the stresses for the third eigenmode

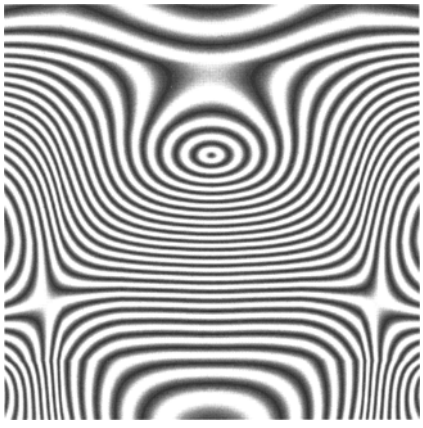

Fig. 4—Isochromatics (the image produced by the circular polariscope) for the third eigenmode

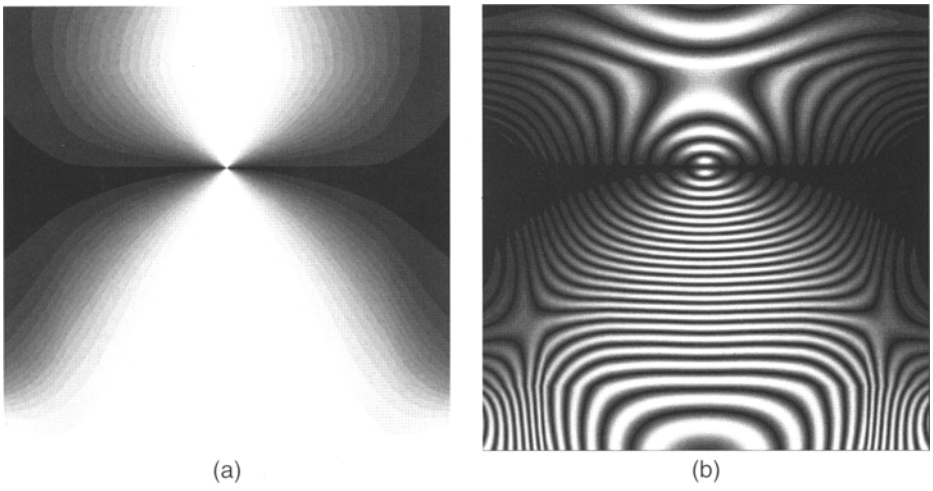

Fig. 5—(a) Image of the isoclinics of the third eigenmode at $\alpha = 0$. (b) Isoclinics and isochromatics intertwined for the third eigenmode at $\alpha = 0$

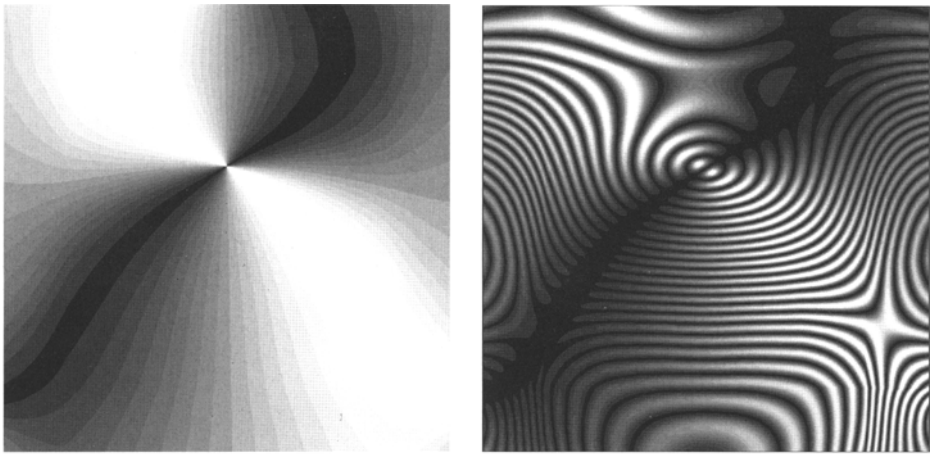

(a) (b)

Fig. 6—(a) Image of the isoclinics of the third eigenmode at $\alpha = \pi/8$. (b) Isoclinics and isochromatics intertwined for the third eigenmode at $\alpha = \pi/8$

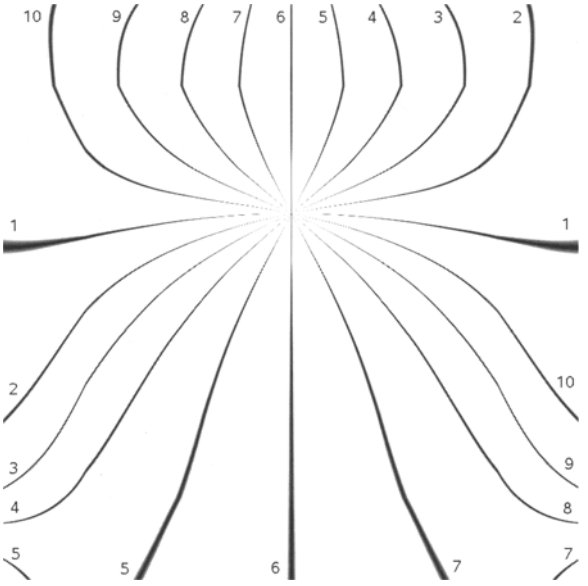

Fig. 7—Isolines of the principal directions of the stresses for the third eigenmode at $\alpha = (i-1)\,\pi/20$, $i = 1, \ldots, 10$

TABLE 1—RELATIONSHIP BETWEEN THE NUMBER OF THE EIGENMODE AND THE NUMBER OF ISOTROPIC POINTS

Number of the eigenmode	1	2	3	4	5	6	7	8
Number of isotropic points	0	0	1	1	5	3	4	8

appropriate smoothing parameter enables the construction of smoothed images of isochromatics (Fig. 8(c)) and isoclinics (Fig. 8(a)).

Concluding Remarks

The generation of digital photoelastic images is not a straightforward procedure. It involves such steps as the construction of a numerical model of the analyzed object, finite element calculations based on the loading scheme and boundary conditions, determination of the nodal vales of stress components and their smoothing, and generation of appropriate digital images. The application of conventional FEA based on a displacement formulation requires the development of special smoothing strategies, and also offers certain advantages. It can be noted that pure experimental photoelastic fringe analysis is concentrated around the reconstruction of the stress fields only. The described procedures can be

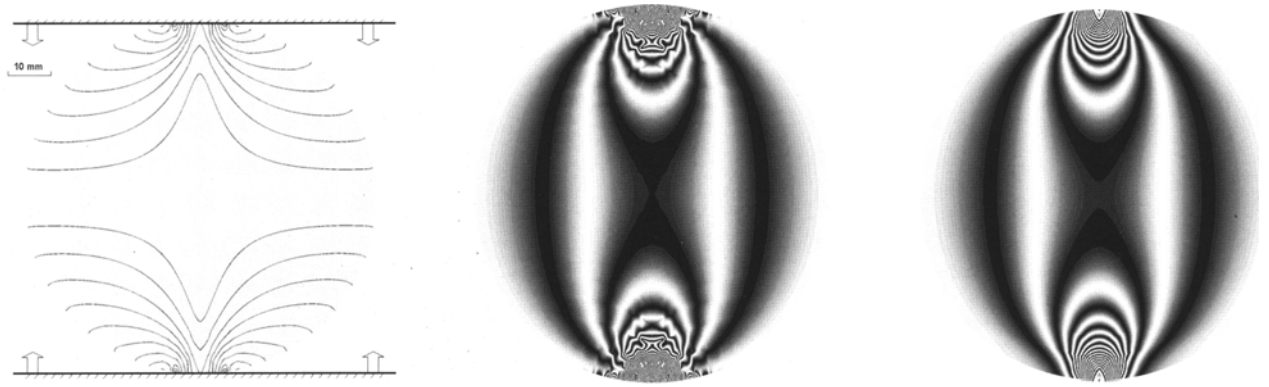

Fig. 8—(a) Loading scheme and pattern of isoclinics of a disk in diametral compression. (b) Unsmoothed isochromatics. (c) Smoothed isochromatics

naturally embedded into hybrid experimental–numerical photoelastic analysis and enable the reconstruction of not only stress but also displacement fields in the analyzed objects.

References

1. Asundi, A. and Sajan, M.R., "Multiple LED Camera for Dynamic Photoelasticity," Applied Optics, **34** *(13), 2236–2240 (1995).*

2. Asundi, A. and Sajan, M.R., "A Low Cost Digital Polariscope for Dynamic Photoelasticity," Optical Engineering, **33**, *3052–3055 (1994).*

3. Pacey, M.N., Haake, S.J., and Patterson, E.A., "A Novel Instrument for Automated Principal Strain Separation in Reflection Photoelasticity," Journal of Testing and Evaluation, **28** *(4), 229–235 (2000).*

4. Timoshenko, S.P. and Goodier, J.N., Theory of Elasticity, Nauka, Moscow (1975).

5. Dally, J.W. and Riley, W.F., Experimental Stress Analysis, McGraw-Hill, New York (1991).

6. Su, X.Y., Asundi, A., and Sajan, M.R., "Phase Unwrapping in Photoelasticity," ICEM'96—Advances and Applications, Singapore (1996).

7. Soifer, V.A., "Computer Processing of Images," Herald of the Russian Academy of Sciences, **71** *(2), 119–129 (2001).*

8. Holstein, A., Salbut, L., Kujawinska, M., and Juptner, W., "Hybrid Experimental–Numerical Concept of Residual Stress Analysis in Laser Weldments," EXPERIMENTAL MECHANICS, **41** *(4), 343–350 (2001).*

9. Segerlind, L.J., Applied Finite Element Analysis, Mir, Moscow (1979).

10. Zienkiewicz, O.C. and Morgan, K., Finite Elements and Approximation, Mir, Moscow (1986).

11. Bathe, K.J., Finite Element Procedures in Engineering Analysis, Prentice-Hall, Englewood Cliffs, NJ (1982).

12. Ramesh, K. and Pathak, P.M., "Role of Photoelasticity in Evolving Discretization Schemes for FE Analysis," Experimental Techniques, **23** *(4), 36–38 (1999).*

13. Atluri, S.N., Gallagher, R.H., and Zienkiewicz, O.C., editors, Hybrid and Mixed Finite Element Methods, Wiley, New York (1983).

14. Ragulskis, M., Maskeliunas R., and Ragulskis L., "Plotting Moire Fringes for Circular Structures from FEM Results," Experimental Techniques, **26** *(1), 31–35 (2002).*

15. Ragulskis M., Palevicius A., and Ragulskis L., "Plotting Holographic Interferograms for Visualization of Dynamic Results From Finite Element Calculations", International Journal for Numerical Methods in Engineering, **56** *(11), 1647–1659 (2003).*